Immunology & Cell Biology 2022; **100**: 312–322
www.wileyonlinelibrary.com/journal/icb

ORIGINAL ARTICLE

OPEN

CXCL11 expressing C57BL/6 mice have intact adaptive immune responses to viral infection

Lennard Dalit[1,2], Carolina Alvarado[1], Lisan Küijper[1], Andrew J Kueh[1,2], Ashley Weir[1,2], Angela D'Amico[1], Marco J Herold[1,2], James E Vince[1,2], Stephen L Nutt[1,2] & Joanna R Groom[1,2]

1 Walter and Eliza Hall Institute of Medical Research, Parkville, VIC, Australia
2 Department of Medical Biology, University of Melbourne, Parkville, VIC, Australia

Keywords
chemokine, germinal center, lung, spleen, T cell differentiation, viral infection

Correspondence
Joanna R Groom, Walter and Eliza Hall Institute of Medical Research, Parkville, VIC 3052, Australia.
E-mail: groom@wehi.edu.au

Present address
Lisan Küijper, Department of Immunopathology, Sanquin, Amsterdam, The Netherlands.
Landsteiner Laboratory, Amsterdam UMC, University of Amsterdam, Amsterdam, The Netherlands.

Received 16 September 2021;
Revised 24 February 2022;
Accepted 26 February 2022

doi: 10.1111/imcb.12541

Immunology & Cell Biology 2022; **100**: 312–322

Abstract

The chemokine receptor CXCR3 is expressed on immune cells to co-ordinate lymphocyte activation and migration. CXCR3 binds three chemokine ligands, CXCL9, CXCL10 and CXCL11. These ligands display distinct expression patterns and ligand signaling biases; however, how each ligand functions individually and collaboratively is incompletely understood. CXCL9 and CXCL10 are considered pro-inflammatory chemokines during viral infection, while CXCL11 may induce a tolerizing state. The investigation of the individual role of CXCL11 *in vivo* has been hampered as C57BL/6 mice carry several mutations that result in a null allele. Here, CRISPR/Cas9 was used to correct these mutations on a C57BL/6 background. It was validated that $CXCL11^{KI}$ mice expressed CXCL11 protein in dendritic cells, spleen and lung. $CXCL11^{KI}$ mice were largely phenotypically indistinguishable from C57BL/6 mice, both at steady-state and during two models of viral infection. While CXCL11 expression did not modify acute antiviral responses, this study provides a new tool to understand the role of CXCL11 in other experimental settings.

INTRODUCTION

Chemokines and their G-protein-coupled receptors play multiple roles in immune homeostasis, inflammation, tumor growth and metastasis, making them promising drug targets in a wide range of diseases.[1] The chemokine superfamily is complex, with most chemokine receptors activated by more than one ligand and many chemokines engaging multiple receptors. Details of ligand hierarchy, signal bias and redundancy are missing for most chemokine receptors. CXCR3 is a pro-inflammatory chemokine receptor that is expressed by subpopulations $CD8^+$ and $CD4^+$ T cells, regulatory T cells, B cells and NK cells, among others.[2,3] During viral infection, CXCR3 is upregulated on antigen-experienced T cells to promote the differentiation of $CD8^+$ short-lived effector and $CD4^+$ helper type 1 (Th1) T cells.[4–8] Following differentiation in lymphoid organs, CXCR3 drives migration of these activated cells to the site of inflammation.[9–11] CXCR3 binds three interferon (IFN)-inducible ligands CXCL9, CXCL10 and CXCL11, that are located on the chromosome 4q21 and share ~40% homology.[12–14] Each CXCR3 ligand gene displays distinct regulatory elements to regulate their expression via Type I and II IFN stimulation.[2,3] Furthermore, each induces individual receptor binding and signaling cascades where CXCL9 and CXCL10 preferentially stimulate G-protein and β-arrestin cascades, while CXCL11 promotes robust calcium flux and receptor desensitization.[3,12,15–18] While this suggests CXCR3 ligands may enact distinct roles,

how each ligand individually contributes during infection is incompletely understood.

Multiple studies show that CXCR3 ligands can directly or indirectly influence $CD4^+$ and $CD8^+$ T cell fate decisions.[4,8,17,19] During dynamic immune responses, memory and newly activated T cells migrate into distinct lymphoid niches.[8] This migration is directed by either CXCL9, CXCL10 or through the collaboration of both ligands.[4,20–22] Further, CXCR3 promotes the migration of NK cells within lymphoid tissues, which can in turn impact T cell differentiation.[23] Although CXCL11 binds CXCR3 with the highest affinity and is expressed in humans and in some mouse strains, the investigation of CXCL11 biology has been hampered as C57BL/6 mice contain several mutations resulting in a null CXCL11 allele.[3,12,15,18,24,25] In addition to CXCR3, CXCL11 binds the atypical chemokine receptor ACKR3 (previously known as CXCR7). ACKR3 binds an additional ligand, CXCL12 (SDF1a) which also binds CXCR4.[26–29]

In contrast to the pro-inflammatory roles of CXCL9/10, it has been proposed that CXCL11 may act to restrain effector T cell differentiation and tumor growth and metastasis.[17,25,30–32] The distinct signaling and expression of CXCL11, the individual functions ascribed to CXCL9 and CXCL10, combined with the lack of tools to guide CXCL11 research, have led to longstanding questions on the role of CXCL11 in the context of inflammation and cancer. Here CRISPR/Cas9 technology was used to correct the mutations found in C57BL/6 mice, to allow us to definitively test the role of CXCL11 during viral infection. $CXCL11^{KI}$ mice were shown to be largely phenotypically indistinguishable from C57BL/6 mice that lack CXCL11 expression, both during steady-state and during two viral infection models. This study establishes that CXCL9 and CXCL10 are the dominant CXCR3 chemokine ligands in the context of viral infection and establishes a validated *in vivo* model to study unexplored roles of CXCL11.

RESULTS

Generation and validation of a CXCL11 mouse on a C56BL/6 background

CXCL11 binds both CXCR3 and ACKR3 and shares these receptors with CXCL9, CXCL10 and CXCL12 (Figure 1a). Understanding the specific roles of CXCL11 has been limited as the inbred strain that is most commonly used in biomedical research, C57BL/6 mice, contain mutations that introduce a premature stop codon in the CXCL11 coding region, resulting in a null allele (Figure 1b).[3,25] To better understand the function of CXCL11 *in vivo*, we generated the $CXCL11^{KI}$ strain using CRISPR/Cas9 technology to restore CXCL11 expression on a C57BL/6 background (Figure 1c and Methods). To validate $CXCL11^{KI}$ mice, we differentiated steady-state dendritic cell (DC) populations *in vitro* from $CXCL11^{KI}$ and $CXCL11^{B6}$ bone marrow precursors. Cultures were stimulated with TLR ligands IMQ, R848 or CpG, which have been shown to induce CXCL9 and CXCL10.[33] DC culture supernatant was analyzed for CXCL11 expression by ELISA (Figure 1d). This confirmed that CXCL11 was produced exclusively by $CXCL11^{KI}$ DC populations in an expected manner.

Steady-state $CXCL11^{KI}$ mice display minor alterations in B and T cell populations and CXCR3 receptor expression

To characterize $CXCL11^{KI}$ mice, we first analyzed the populations of B and conventional $CD8^+$ and $CD4^+$ T cells in the spleens of adult animals. A small but consistent decrease in the frequency of $B220^+$ cells and a reciprocal increase in $CD8^+$ T cells was observed in $CXCL11^{KI}$ mice (Figure 2a, b). However, this resulted in only a minor increase in the total number of splenic $CD8^+$ T cells, with no significant differences found in $B220^+$ or conventional $CD4^+$ T cell numbers (Figure 2b). Previous studies have demonstrated that, unlike CXCL9 and CXCL10, the production of CXCL11 may induce a tolerizing state.[17] However, we found that the frequency and number of $FoxP3^+CD4^+$ T regulatory cells were comparable in $CXCL11^{KI}$ and control mice (Figure 2c, d). We next investigated the level of steady-state activation and the expression of CXCR3 (Figure 2e). We found the frequency of CXCR3 was reproducibly lower in conventional $CD4^+$ ($FoxP3^-$) T cells, while this was not observed in other populations, such as B cells, $CD8^+$ and T regulatory cells (Figure 2f). As CXCL11 binds CXCR3 with the highest affinity and leads to increased receptor internalization, it is possible that this decreased frequency of CXCR3 in $CXCL11^{KI}$ conventional $CD4^+$ cells was a result of increased ligand expression.[12,15,18] However, within the $CXCR3^+CD4^+$ T cell population, the mean fluorescence of CXCR3 detection was comparable in $CXCL11^{KI}$ and $CXCL11^{B6}$ animals, suggesting a different mechanism for the observed difference in the frequency of CXCR3 expression. Combined, this work demonstrates that $CXCL11^{KI}$ and litter mate control $CXCL11^{B6}$ mice are largely alike in their adaptive immune compartments without infection.

Effector and memory T cell differentiation is intact in $CXCL11^{KI}$ mice following viral infection

The CXCR3 ligands expressed in C57BL/6 mice display distinct roles for the positioning of T cells following

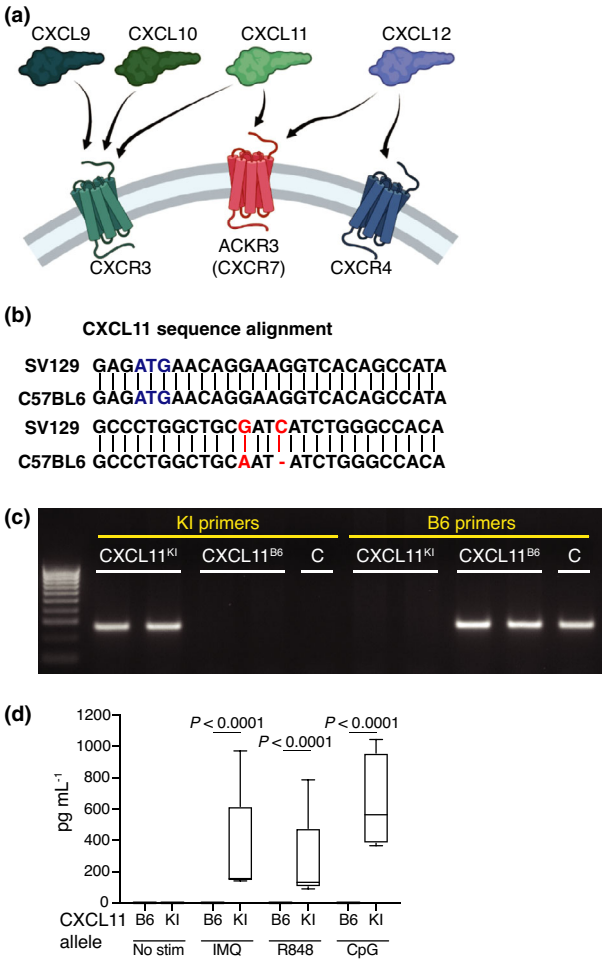

Figure 1. CXCL11^{KI} mice generated by CRISPR/Cas9 technology contain nontruncated CXCL11 sequence and express CXCL11 protein. **(a)** Scheme of receptor–ligand interactions of CXCL11 and related chemokines. **(b)** Alignment of WT (strain SV129) and C57BL/6 CXCL11 gene sequences. Start codon (blue) and allele variation (red) mice resulting in a silent mutation at amino acid 12 and a frameshift mutation from amino acid 13 leading to the absence of the CXCL11 protein. **(c)** PCR genotyping gel of CXCL11^{B6} or CXCL11^{KI} DNA with CXCL11^{KI} and CXCL11^{B6} primers. C indicates known C57BL/6 allele DNA. **(d)** CXCL11 protein production in CXCL11^{B6} and CXCL11^{KI} DC cultures stimulated for 5 h with IMQ, R848, or CpG, determined by ELISA. Data are representative of two independent experiments of 4 mice per group. Data are median and minimum and maximum data points.

acute lymphocytic choriomeningitis virus (LCMV) challenge. Specifically, during primary or recall challenge, CXCL9 and CXCL10 can act independently to promote T cell relocation for CD8$^+$ effector populations.[8,21] We therefore used the acute LCMV system to determine the role for CXCL11 in T cell differentiation towards effector and memory populations. We first confirmed that CXCL11 expression is induced following infection. This identified high CXCL11 expression in splenic protein extracts from CXCL11^{KI} mice 4 days post LCMV infection (Figure 3a). In comparison, the levels of CXCL11 in the serum were considerably lower and no CXCL11 protein was detected in CXCL11^{B6} mice (Figure 3b). As the expression of CXCL9 and CXCL10 within lymphoid organs is upregulated prior to their influence on T cell effector function being detected, we evaluated the role of CXCL11 protein production within the spleen D8 following LCMV infection.[8,21] At this time, CXCL11^{KI} and CXCL11^{B6} mice displayed similar frequencies and total cell numbers of splenic polyclonal short-lived effector (CD44$^+$KLRG1$^+$CD62L$^-$) and memory precursor (CD44$^+$KLRG1$^-$CD62L$^+$) populations (Figure 3c–e). To compare this response within T cells of known antigen specificity, we used an MHC I tetramer to detect GP33-specific and NP396-specific cells (Figure 3f, g). We found both GP33- and NP-396-specific CD8$^+$ T cells expanded and formed effector and memory populations that were indistinguishable between CXCL11^{KI} and CXCL11^{B6} mice (Figure 3h–j and data not shown). Similar to CD8$^+$ T cells, CD4$^+$ T cells also rely on CXCR3 for the formation of effector Th1 cells.[4] However, we found no significant role for *in vivo* CXCL11 expression in either the polyclonal or antigen-specific differentiation (detected by MHC II tetramers specific for GP66) of Th1 (CD44$^+$Ly6C$^+$CD162$^+$) cells in C57BL/6 mice following LCMV challenge (Figure 3k–q). Combined, this work indicates that unlike CXCL9 and CXCL10, CXCL11 expression does not overtly alter effector T cell differentiation following LCMV infection.

Germinal center responses are unaffected by CXCL11 expression during LCMV challenge

In addition to the well-established role for CXCR3 in directing T cell effector function and location, CXCR3 and the expression of its key transcriptional regulator, T-bet, can also influence the formation and function of T follicular helper (Tfh) and germinal center (GC) B cells.[34–36] Further, as CXCL11 links CXCR3 and CXCR4 chemokine families through binding ACKR3, we reasoned that expression of CXCL11 may influence GC B cell responses by modulating CXCL12 and CXCR4 signaling.[24,26,28,31,37] We therefore investigated the contribution of CXCL11 to the formation of Tfh and GC B cells and immunoglobulin isotype switching following viral infection. We found no role for CXCL11 in polyclonal or GP66 antigen-specific differentiation of Tfh (CD44$^+$Ly6C$^-$CD162$^-$CXCR5$^+$CD279$^+$) cells D8 following LCMV infection (Figure 4a–e). Following infection, the number of splenic B cells was comparable between

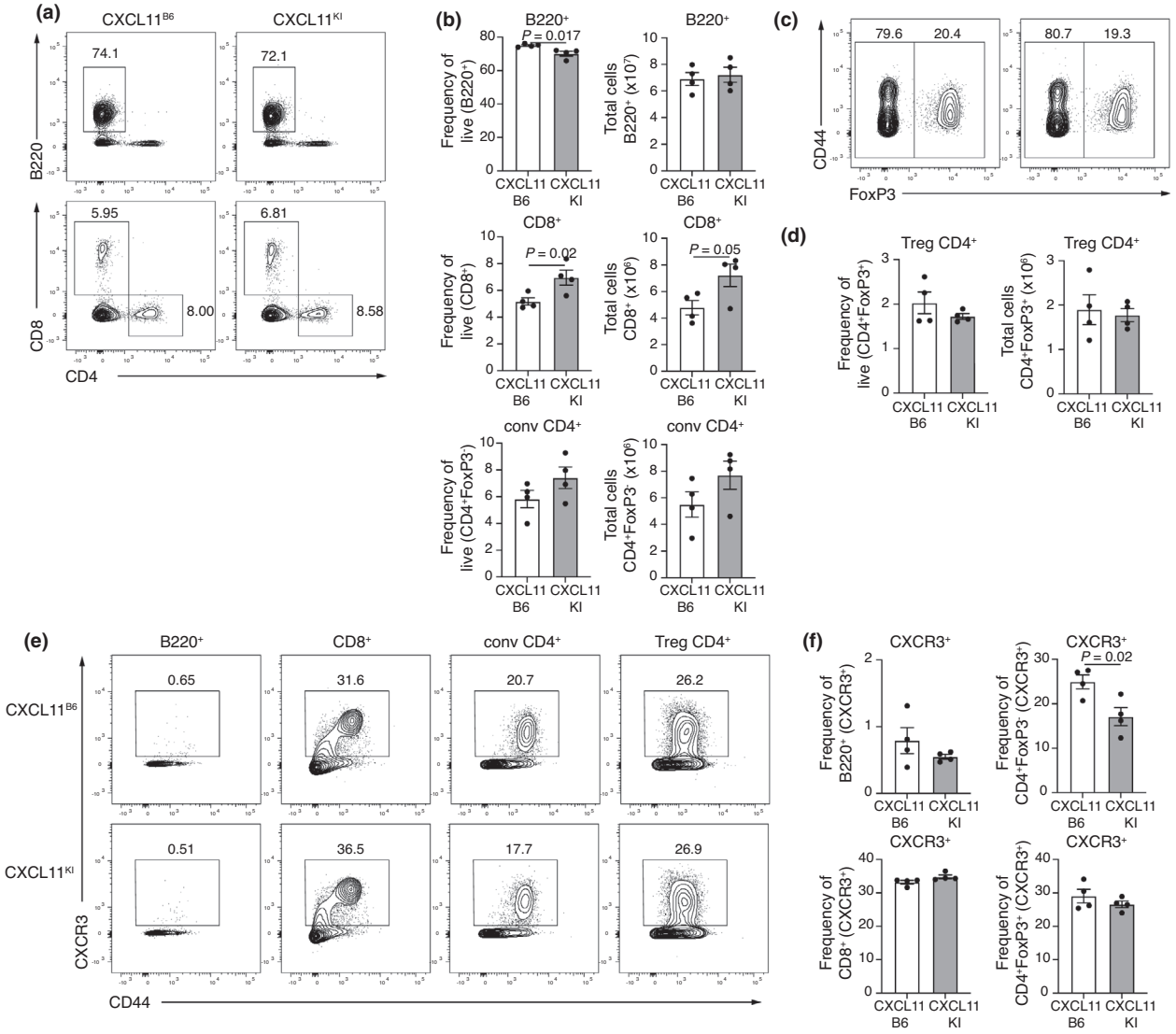

Figure 2. Steady-state CXCL11 expression results in minor alteration in B and T cell populations and CXCR3 receptor expression *in vivo*. $CXCL11^{B6}$ and $CXCL11^{KI}$ splenocytes were harvested at steady-state from uninfected adult mice. **(a)** Representative plots and **(b)** frequency and total numbers of $B220^+$ B cells, conventional (conv, $CD4^+FoxP3^-$) $CD4^+$ T cells, and $CD8^+$ T cells from $CXCL11^{B6}$ or $CXCL11^{KI}$ splenocytes. **(c)** Representative plots and **(d)** frequency and total numbers of T_{reg} ($CD4^+FoxP3^+$) in $CXCL11^{B6}$ or $CXCL11^{KI}$ mice. **(e)** Representative plots and **(f)** frequency of $CXCR3^+$ expression in $B220^+$ B cells, $CD8^+$ T cells, conv $CD4^+$ T cells, and regulatory T cells (T_{reg}) in $CXCL11^{B6}$ or $CXCL11^{KI}$ mice. Data are representative of three independent experiments of 3–5 mice per group. Data are mean ± s.e.m.

$CXCL11^{KI}$ and $CXCL11^{B6}$ mice (Figure 4f). Similarly, the formation of GC B ($B220^+CD38^-IgD^-CD95^+$) cells was intact in $CXCL11^{KI}$ animals (Figure 4g–i). During viral infections, T-bet acts in a cell-type specific manner to steer heavy chain usage away from IgG1 and towards IgG2a/c usage in $CXCL11^{B6}$ (wildtype C57BL/6) mice.[38] Recently, this process has been shown to occur in a T-bet directed niche, which promotes T–B cell interactions in a CXCR3-dependent manner.[39] Both CXCL9 and CXCL10 have been shown to be expressed near the T-B border and within the B cell follicle of draining lymph nodes.[4,39,40] We found this process was not further influenced by CXCL11 expression, as similar surface levels of IgG1 and IgG2a/c isotypes were present on GC B cells in $CXCL11^{KI}$ and $CXCL11^{B6}$ mice following LCMV infection (Figure 4j–l). Collectively, with the data presented above (Figures 3 and 4), these studies demonstrate that adaptive immune responses are not impacted by CXCL11 expression in response to LCMV infection.

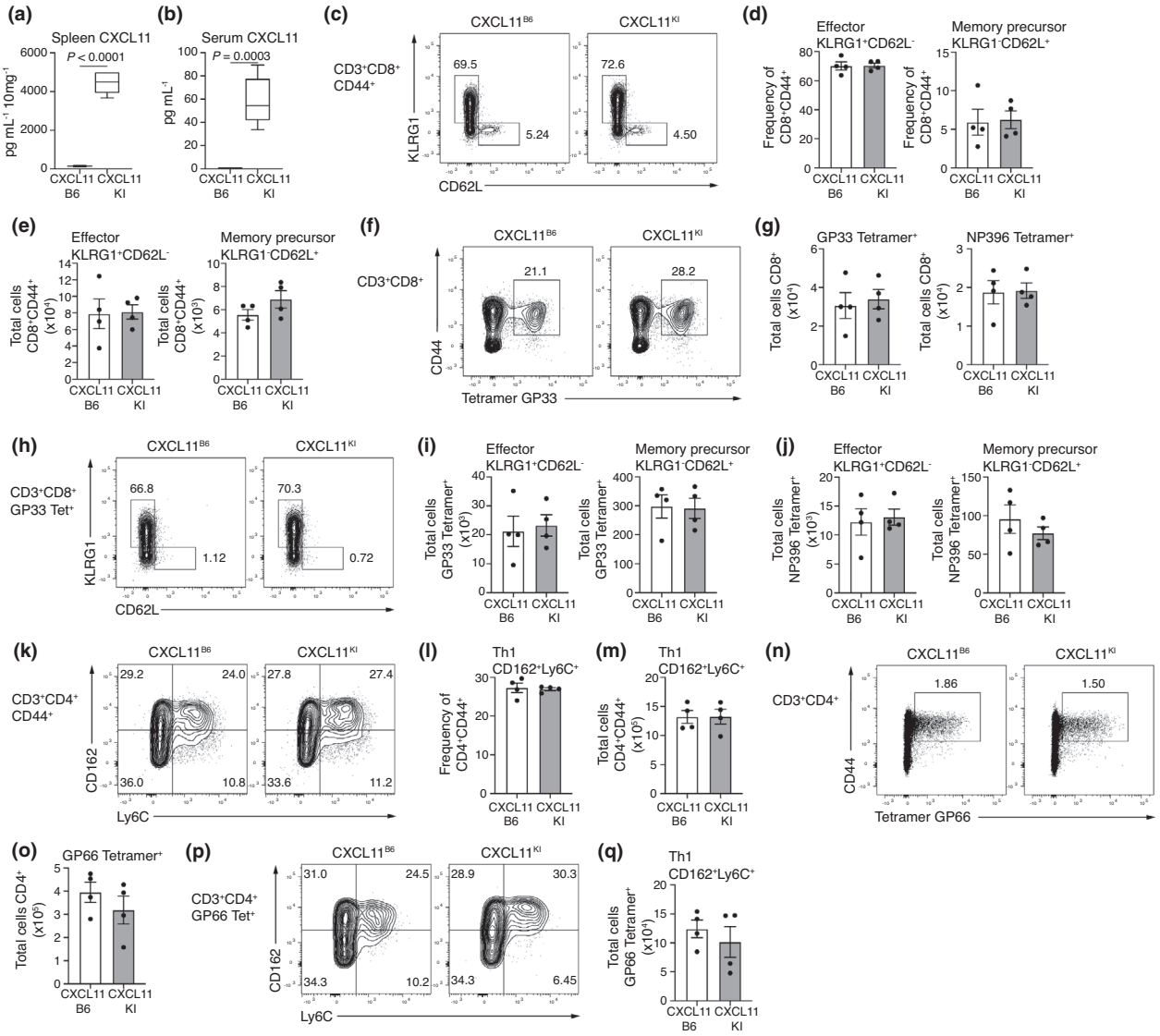

Figure 3. Lymphocytic choriomeningitis virus (LCMV) infected CXCL11^{KI} mice display intact effector and memory T cell differentiation. **(a, b)** CXCL11 protein in **(a)** spleen tissue lysates and **(b)** serum from CXCL11^{B6} and CXCL11^{KI} mice 4 days following LCMV infection. Data are median, minimum and maximum of 5 mice per group. **(c–q)** Splenocytes were analyzed from CXCL11^{B6} and CXCL11^{KI} mice D8 following LCMV infection. **(c)** Representative plots and **(d)** frequency and **(e)** total numbers of CD8$^+$ effector (CD44$^+$KLRG1$^+$CD62L$^-$) and memory precursor (CD44$^+$KLRG1$^-$CD62L$^+$) in CXCL11^{B6} and CXCL11^{KI} cells. **(f)** Representative plots of GP33 tetramer$^+$CD44$^+$ cells and **(g)** total numbers of GP33 and NP396 tetramer$^+$CD44$^+$ cells. **(h)** Representative plots and **(i,j)** total numbers of effector (CD44$^+$KLRG1$^+$CD62L$^-$) and memory precursor (CD44$^+$KLRG1$^-$CD62L$^+$) in **(i)** GP33 and **(j)** NP396 tetramer$^+$CD44$^+$ CD8$^+$ cells. **(k)** Representative plots and **(l)** frequency and **(m)** total numbers of CD4$^+$ Th1 (CD44$^+$CD162$^+$Ly6C$^+$) in CXCL11^{B6} and CXCL11^{KI} cells. **(n)** Representative plots and **(o)** total numbers of GP66 tetramer$^+$CD44$^+$ cells. **(p)** Representative plots and **(q)** total numbers of CD4$^+$ Th1 (CD44$^+$CD162$^+$Ly6C$^+$) in GP66 tetramer$^+$CD44$^+$ cells. Data are representative of three independent experiments of 3–5 mice per group. Data are mean ± s.e.m.

Intact T cell responses following influenza infection

Distinct viral infections can perturb the adaptive immune response in a pathogen-specific manner. We and others have demonstrated that LCMV induces a highly inflammatory environment within secondary lymphoid tissues, which impacts the transcriptional regulators that underpin T cell differentiation.[38,41] Critically, LCMV infection induces high levels of both CXCL9 and CXCL10.[8,41] We reasoned that the overwhelming inflammation which occurs during LCMV infection may lead to compensation between CXCR3 ligands and result

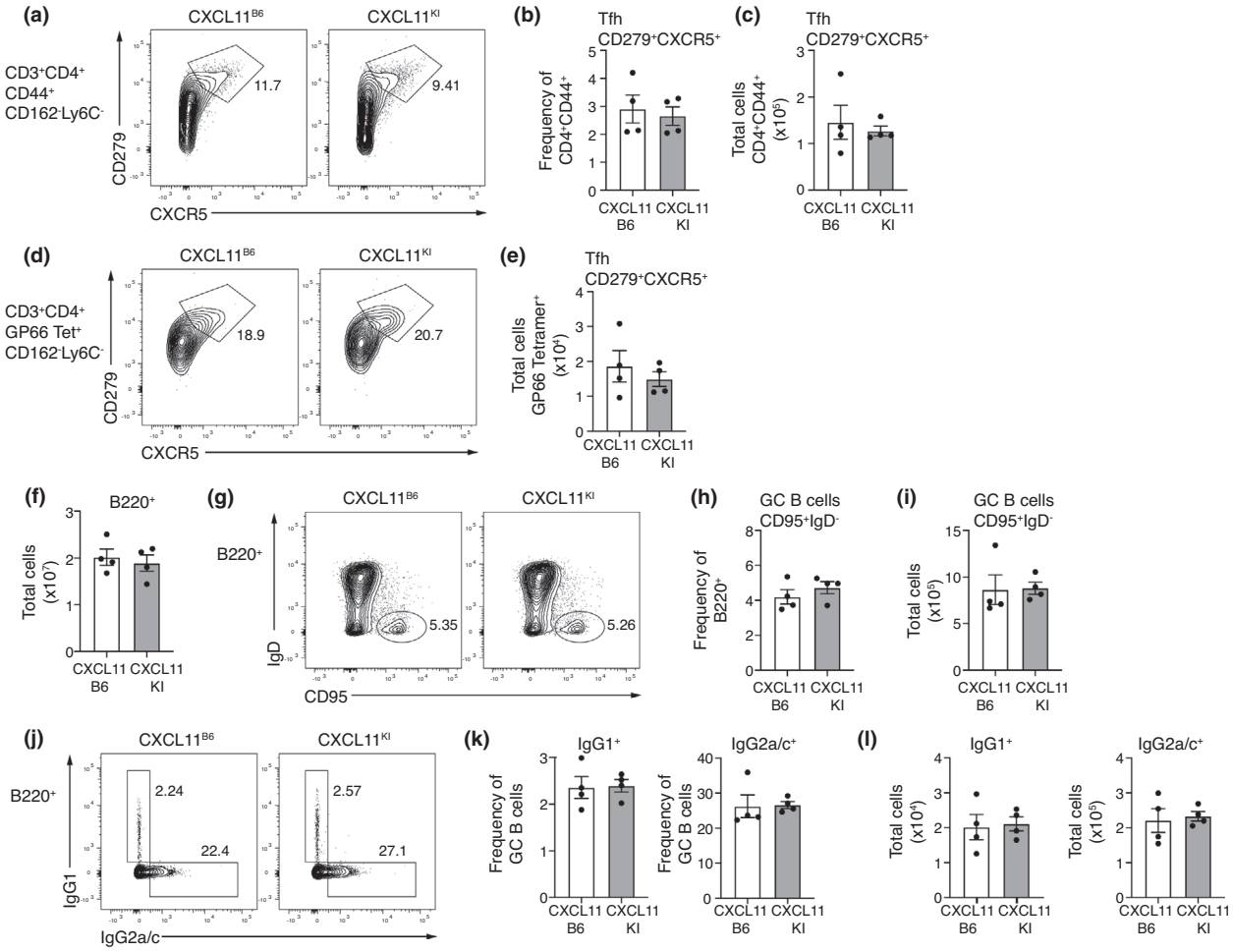

Figure 4. Lymphocytic choriomeningitis virus (LCMV) infected CXCL11^{KI} mice exhibit an intact germinal center response. Splenocytes were analyzed from CXCL11^{B6} and CXCL11^{KI} mice D8 following LCMV infection. **(a)** Representative plots and **(b)** frequency and **(c)** total numbers of CD4$^+$ Tfh (CD44$^+$CD162$^-$Ly6C$^-$CD279$^+$CXCR5$^+$) in CXCL11^{B6} and CXCL11^{KI} cells. **(d)** Representative plots and **(e)** total numbers of Tfh (CD44$^+$CD162$^-$Ly6C$^-$CD279$^+$CXCR5$^+$) GP66 tetramer$^+$CD44$^+$ cells. **(f)** Total numbers of B220$^+$ B cells in CXCL11^{B6} and CXCL11^{KI} mice. **(g)** Representative plots, **(h)** frequency and **(i)** total numbers of GC B cells (B220$^+$IgD$^-$CD95$^+$). **(j)** Representative plots, **(k)** frequency and **(l)** total numbers of IgG1$^+$ and IgG2a/c$^+$ GC B cells in CXCL11^{B6} and CXCL11^{KI}. Data are representative of three independent experiments of 3–5 mice per group. Data are mean ± s.e.m.

in a setting where the independent role of CXCL11 is obscured. We next sought to investigate the role of CXCL11 in C57BL/6 mice using a viral infection model that did not directly infect lymphoid tissue and therefore causes less inflammation within secondary lymphoid organs.[38] Consistent with this hypothesis, CXCL11 was expressed in the spleen of CXCL11^{KI} mice intranasally with influenza (X31 strain), albeit at a lower concentration than that observed post LCMV (Figures 5a and 3a). Similar to what we observed during LCMV infection, on D8 of influenza infection the differentiation of splenic CD8$^+$ effector and memory formation for the polyclonal and individual NP366 antigen-specific populations was not statistically different between CXCL11^{KI} and CXCL11^{B6} mice (Figure 5b, c). This was matched when investigating the polyclonal and NP311 antigen-specific CD4$^+$ T cell differentiation towards both Th1 and Tfh cells (Figure 5d, e). Further, we found no significant role for CXCL11 expression in the differentiation of GC B cells, or IgG1 and IgG2a/c isotype usage on GC B cells during influenza infection (Figure 5f, g). Consistent with this, GC structures formed in spleens following influenza infection were indistinguishable between CXCL11^{KI} and CXCL11^{B6} animals (Figure 5h). As CXCL11 had an insignificant role on the differentiation of T and B cells, we questioned whether a

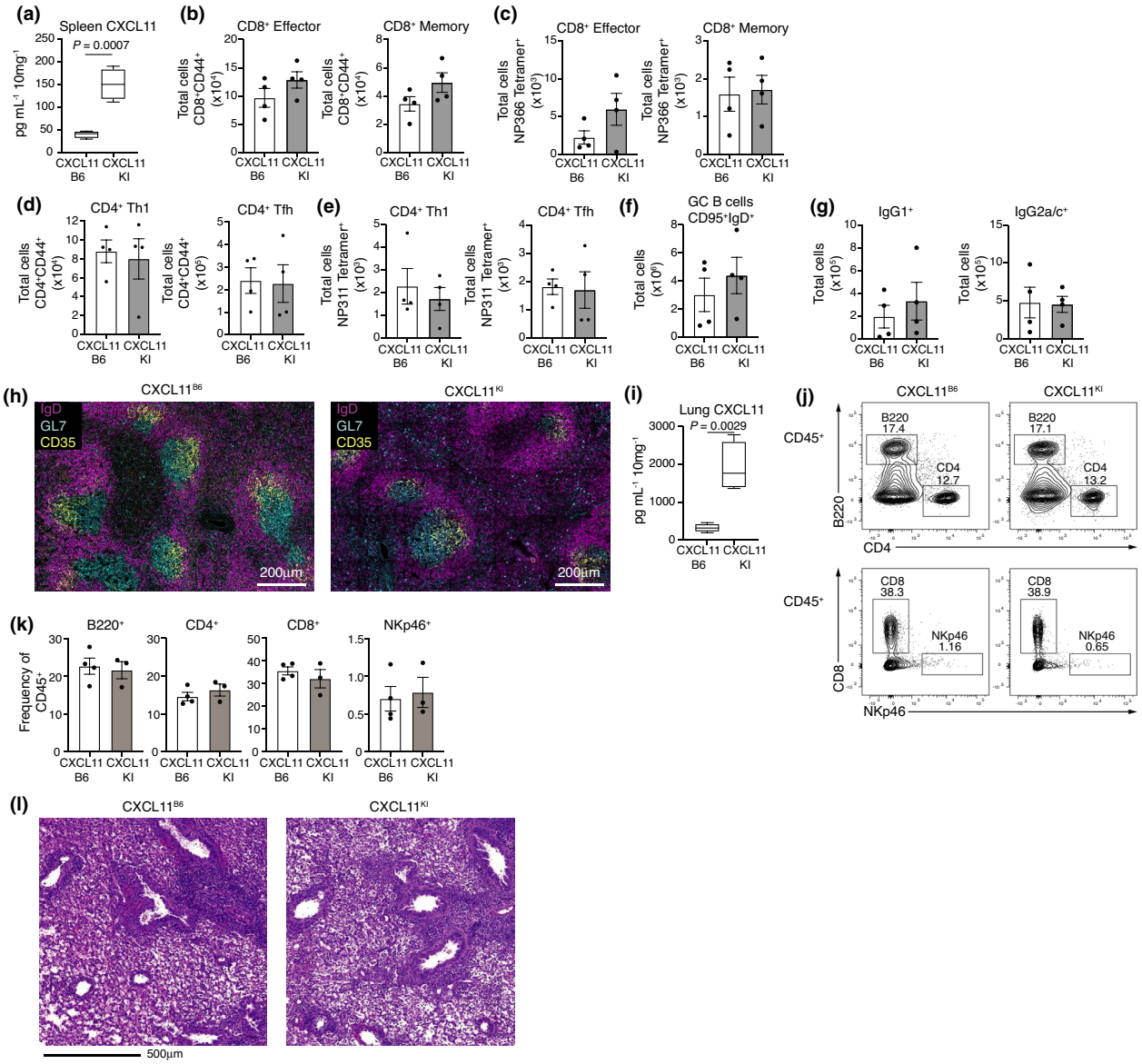

Figure 5. Polyclonal and antigen-specific response to influenza A remains intact in CXCL11^{KI} mice. **(a)** CXCL11 protein in spleen tissue lysates from CXCL11^{B6} and CXCL11^{KI} mice 4 days following influenza infection. Data are median, minimum and maximum of 5 mice per group. **(b–h, j–l)** CXCL11^{B6} and CXCL11^{KI} mice were analyzed D8 following influenza infection. **(b, c)** Total numbers of splenic CD8$^+$ effector (CD44$^+$KLRG1$^+$CD62L$^-$) and memory precursor (CD44$^+$KLRG1$^-$CD62L$^+$) **(b)** polyclonal and **(c)** NP366 tetramer$^+$ cells in CXCL11^{B6} and CXCL11^{KI} mice. **(d, e)** Total numbers of splenic CD4$^+$ Th1 (CD44$^+$CD162$^+$Ly6C$^+$) and Tfh (CD44$^+$CD162$^-$Ly6C$^-$CD279$^+$CXCR5$^+$) **(d)** polyclonal and **(e)** NP311 tetramer$^+$ cells in CXCL11^{B6} and CXCL11^{KI} mice. **(f)** Total numbers of splenic GC B cells (B220$^+$IgD$^-$CD95$^+$) and **(g)** total numbers of IgG1$^+$ and IgG2a/c$^+$ GC B cells in CXCL11^{B6} and CXCL11^{KI}. **(h)** Representative confocal micrographs of splenic GCs D8 of CXCL11^{B6} and CXCL11^{KI} mice stained with IgD (magenta, follicle), GL7 (cyan, GC structure) and CD35 (yellow, follicular dendritic cell stain). The scale bar represents 200 µm. **(i)** CXCL11 protein expression in lung tissue lysates from CXCL11^{B6} and CXCL11^{KI} mice 4 days following influenza infection. Data are median, minimum and maximum of 5 mice per group. **(j)** Representative plots and **(k)** frequency of B220$^+$ B cells, CD4$^+$ and CD8$^+$ T cells, and NKp46$^+$ NK cells in CD45$^+$ cells infiltrating the lung parenchyma of CXCL11^{B6} and CXCL11^{KI}. **(l)** Representative immunohistochemistry staining of lung tissue sections CXCL11^{B6} and CXCL11^{KI} mice. The scale bar represents 500 µm. Data are representative of three independent experiments of 3–5 mice per group. Data are mean ± s.e.m.

distinct role could be elucidated by assessing the cellular migration to an inflamed peripheral site. Previously, in a non-infectious setting, intratracheal delivery of CXCL11 led to the recruitment of activated T cells into the lung.[9] The use of influenza provided a system where CXCL11 protein was expressed in the lung in CXCL11^{KI}, ensuring

that a role for CXCL11-directed migration to the lung could be assessed directly (Figure 5i). The frequencies of $B220^+$, $CD4^+$, $CD8^+$ and NK cells were determined in perfused lungs D8 following influenza infection. Although CXCR3 has previously been shown to impact lung T cell migration, we saw no difference in the ratios of immune cells within the lung parenchyma between $CXCL11^{KI}$ and $CXCL11^{B6}$ mice (Figure 5j, k). Similarly, comparable lung histology was observed between CXCL11 expressing and C57BL/6 animals (Figure 5l). Therefore, CXCL11 expression seemed not to make an important contribution to the differentiation, function or migration of immune cells following influenza infection.

DISCUSSION

Despite validating the expression of CXCL11 in DCs, spleen and lung tissue from $CXCL11^{KI}$ animals, we showed no independent role for CXCL11 in two distinct viral infection models on a C57BL/6 background. Given the importance of CXCR3 in orchestrating immune cell differentiation, function and migration, identifying a null phenotype in CXCL11-expressing C57BL/6 mice is surprising but answers a longstanding question for a major inflammatory system. Previous work has demonstrated distinct roles for both CXCL9 and CXCL10 using individual knockouts for each ligand.[3,4,8,21] In contrast, this study demonstrated an unappreciated level of redundancy between the CXCR3 ligands, such that the addition of CXCL11 on the C57BL/6 background did not demonstrate variation in adaptive responses against two viral infection models. These results contrast with previous studies that suggest that the differential expression of functional CXCL11 between mouse strains may account for distinct susceptibility to infectious pathogens.[25] Further, given that the antiviral responses of $CXCL11^{KI}$ mice were parallel to those observed in litter mate controls, we failed to reveal any evidence of increased T cell suppressor function, as has been indicated with CXCL11-Fc treatments.[17] This distinction potentially reflects differences in the level of CXCL11 gene expression due to the genomic modification performed here, rather than higher concentrations that may be achieved with CXCL11-Fc treatment.

Importantly, the established knockout lines for CXCL9 and CXCL10 carry passenger mutations derived from the 129 embryonic stem cells used in their generation.[42–44] Thus, the generation of $CXCL11^{KI}$ mice provides an appropriate control line for these widely used lines. Further, our observation that steady-state immune development and antiviral responses are largely unaffected by the physiological expression of CXCL11 is consistent with work that has directly compared CXCL9 and CXCL10 knockout animals and observed distinct roles.[4,8,19] Further work is needed to establish whether CXCL11 has a discernible function during viral infection in the absence of both CXCL9 and CXCL10.

As the induction and role of CXCR3 is context-dependent, there are likely to be other experimental settings in which an independent role for CXCL11 expression may be found. The new, validated animal model described herein, will be important to assess experimentally the role of CXCL11 and cross-talk between CXCR4 and ACKR3 in these settings.[32] Of particular interest will be the investigation of cancer types in which CXCL11 over-expression correlates with tumor progression.[45] Further, investigation of gain-of-function CXCR4 mutations on a $CXCL11^{KI}$ background may more reliably phenocopy the rare immunodeficiency, WHIM syndrome, as this new model more fully recapitulates the complexity of the human chemokine system.[46]

METHODS

Mice and viral infections

Mice were maintained on a C57BL/6 background in specific-pathogen-free conditions. Animal experiments were performed in accordance with the WEHI animal ethics committee. The $CXCL11^{KI}$ mice were generated by the WEHI MAGEC laboratory on a C57BL/6J background. To generate $CXCL11^{KI}$ mice, 20 ng μL^{-1} of *Cas9* mRNA, 10 ng μL^{-1} of sgRNA and 40 ng μL^{-1} of the oligo donor (Supplementary table 1) were injected into the cytoplasm of fertilized one-cell stage embryos generated from wild-type C57BL/6J breeders. Twenty-four hours later, two-cell stage embryos were transferred into the uteri of pseudo-pregnant female mice. Viable offspring were genotyped by next-generation sequencing. Targeted animals were backcrossed twice to wild-type C57BL/6J to eliminate off-target mutations. To genotype, DNA was amplified for 34 cycles using specific primers (Supplementary table 2). Littermates matched for gender and age (6–10 weeks of age) were used as controls in this study. Mice were infected intravenously with 3×10^3 PFU LCMV Armstrong or intranasally with 1×10^4 PFU influenza virus strain HKx31 (H3N2). For influenza-infected mice, the animals were perfused with PBS to clear circulating lymphocytes prior to analysis.

CXCL11 ELISA on DC supernatants and tissue lysates

Flt3-ligand DCs were generated as described previously.[33] Briefly, bone marrow was flushed and washed in RPMI1640 3% fetal calf serum (FCS), through a FCS underlay. Red cells were removed, and the cells were washed twice through a FCS underlay. The cells were cultured at 1.5×10^6 cells mL^{-1} in specific DC-media (KDS RPMI, 2-ME, 10% FBS) containing 200 ng mL^{-1} recombinant Flt3-ligand (BioXCell, Lebanon, NH, USA) for D8 at 37°C in 10% CO_2. Flt3-ligand

DCs were resuspended in cultured DC-media at a concentration of 5×10^5 cells mL^{-1} and cultured alone or with 1 μg mL^{-1} IMQ, R848 or CpG (InVivoGen, San Diego, CA, USA) for 5 h at 37°C in 10% CO_2. The spleens and lungs were harvested from 4-day infected mice and snap frozen on dry ice. The tissue was weighed, cut and digested with 10 μL mg^{-1} DISC lysis buffer (20 mM Tris-HCl pH 7.5, 150 mM NaCl, 2 mM EDTA, 1% TritonX-100, 10% glycerol, H_2O, protease inhibitor cocktail tablet: Roche, Basel, Switzerland). The tissue was lysed with TissueLyser85300 (Qiagen, Hilden, Germany) and the supernatant was collected between the pellet and fat layers following a 20 000 *g* 15 min spin. Supernatant from cultures, protein lysates, and serum were loaded onto a CXCL11 ELISA kit. A mouse I-TAC/CXCL11 ELISA kit (Sigma-Aldrich, St Louis, MO, USA) was used as per the manufacturer's instructions with culture supernatant incubated 2 h at room temperature (RT) or overnight at 4°C. The plates were washed four times and incubated with biotinylated detection antibody for 1 h at RT with gentle shaking. The plates were washed four times and incubated with streptavidin-HRP for 45 min at RT with gentle shaking. The plates were washed four times and incubated with TMB one-step substrate reagent in the dark for 30 min to develop. Stop solution was added and the absorbance at 450 nm was read using a plate reader (BMG Labtech, Ortenberg, Germany).

Cell preparation and flow cytometry

The tissues were mechanically dissociated to single cell suspensions and enriched for $CD4^+$ or $CD8^+$ T cells as described previously to enrich T cell lineages.[38] Antibody-bound cells were removed by negative selection using BioMag Goat anti-Mouse/anti-Rat IgG beads (Qiagen). The enriched cells were stained with tetramers to detect antigen-specific LCMV ($GP_{66\text{-}77}$:1-A^b, GP_{33}: H-2D^b and NP_{396}:H-2D^b) and influenza A ($NP_{311\text{-}325}$:1-A^b and $NP_{366\text{-}374}$: H-2D^b) responses respectively, that were obtained from NIH tetramer facility and as a gift from J.J. Moon. The cells were stained using indicated antibodies for 20 min at 4°C, followed by fixable viability stain (a700, BD Biosciences, Franklin Lakes, NJ, USA) for 10 min at 4°C, and intracellular proteins were detected using a Foxp3 staining kit according to the manufacturer's protocol (BioLegend, San Diego, CA, USA). *For T cell analysis*: anti-CD45 (clone 30-F11), anti-CD3 (clone 145-2C11), anti-CD8a (clone 53-6.7), anti-KLRG1 (clone 2F1), anti-CD44 (clone IM7) anti-CD4 (clone GK1.5), anti-CD162 (clone 2PH1), anti-Ly6C (clone HK1.4), anti-CD62L (clone MEL-14), anti-CD279 (clone RMP1-30), anti-CXCR3 (clone CXCR3-173), anti-CXCR5 (clone L138D7) and anti-FoxP3 (clone FJK-16S) from BioLegend. *For B cell analysis*: anti-B220 (clone RA3-6B2), anti-CD95 (clone JO2), anti-IgG1 (clone X56), IgG2a/b (clone R2-40) and anti-CD138 (clone 281-2) from BD Biosciences, anti-CD38 (clone 90) from eBioscience (San Diego, CA, USA) and anti-IgD (clone 1126c) from WEHI antibody facility. *For NK cell analysis*: Anti-NKp46 (clone 29A1.4) from BioLegend. Flow cytometry analysis was performed on a BD LSRFortessa X-20 cell analyzer (BD Biosciences). Data analysis was performed with FlowJo version.10 (FlowJo LLC, Ashland, OR, USA).

Immunofluorescence and confocal microscopy

The spleens were fixed in 4% paraformaldehyde and immersed in 30% sucrose before being embedded in Tissue-Tek OCT compound (Sakura Finetek, Torrance, CA, USA). The tissues were cut via microtome (Leica Biosystems, Wetzlar, Germany) into 20 μm sections onto Superfrost Plus slides. The sections were blocked in PBS containing 0.1% Triton X-100 (Sigma-Aldrich) and 10% donkey serum (Jackson ImmunoResearch, West Grove, PA, USA) and stained with directly conjugated anti-GL7 (clone GL7, 1/100), anti-IgD (clone 1126c, 1/100) from WEHI antibody facility and CD35 (clone 8C12, 1/100) from BD Biosciences. The slides were washed in 0.1% Triton X-100 PBS and the coverslips were mounted with Prolong Diamond (ThermoFisher Scientific, Waltham, MA, USA). Images were acquired using a LSM780 confocal microscope using a 20× objective (ZEISS Microscopy, Jena, Germany). The acquisition software was Zen Black 2012 (ZEISS Microscopy).

Histology

The lungs were fixed in 10% formalin, paraffin embedded and sectioned via microtome (Leica Biosystems) and H&E stained. Images were acquired using 3DHistech scanning machine 20× brightfield and 3Dhistech CaseViewer software (3DHISTECH, Budapest, Hungary).

Statistical analysis

Graphs were generated using Prism 8 (GraphPad Software, San Diego, CA, USA), and statistical significance was determined by the unpaired two-tailed Student's *t*-test. *P*-values less than 0.05 were considered significant. All graphs depict mean ± s.e.m.

ACKNOWLEDGMENTS

We acknowledge the late Dr Amanda Proudfoot for discussions at the conception of this study and Dr Nicolas Jacquelot for technical help and discussions. The CXCR3 ligand scheme was generated using Biorender. $CXCL11^{KI}$ mice were generated by the WEHI MAGEC laboratory supported by Phenomics Australia and the Australian Government through the National Collaborative Research Infrastructure Strategy (NCRIS) program. This work was supported by National Health and Medical Research Council (NHMRC) Investigator grant (2007812), Ideas grant (1182649) and Project grant (1137989) grants to JRG. LD is supported by Melbourne research scholarships. JRG was supported by Australian Research Council Future Fellowship (FT130100708) and WEHI Centenary Fellowship sponsored by CSL. JEV was supported by an NHMRC Ideas grant (1183070) and fellowship (1141466). MJH is supported by the Leukemia and

Lymphoma Society of America (LLS SCOR 7015-18) and NHMRC Ideas Grant (118657). This work was made possible through Victorian State Government Operational Infrastructure Support and Australian Government NHMRC IRIISS. Open access publishing facilitated by The University of Melbourne, as part of the Wiley – The University of Melbourne agreement via the Council of Australian University Librarians.

CONFLICT OF INTEREST

The authors declare no conflict of interest.

AUTHOR CONTRIBUTIONS

Lennard Dalit: Formal analysis; Investigation; Methodology; Visualization; Writing – original draft. **Carolina Alvarado:** Formal analysis; Investigation. **Lisan Kuijper:** Formal analysis; Investigation. **Andrew J Kueh:** Investigation; Methodology. **Ashley Weir:** Investigation. **Angela D'Amico:** Investigation. **Marco J Herold:** Resources. **James E Vince:** Resources. **Stephen L Nutt:** Resources. **Joanna R Groom:** Conceptualization; Data curation; Formal analysis; Funding acquisition; Resources; Supervision; Visualization; Writing – original draft.

REFERENCES

1. Griffith JW, Sokol CL, Luster AD. Chemokines and chemokine receptors: positioning cells for host defense and immunity. *Annu Rev Immunol* 2014; **32**: 659–702.
2. Groom JR. Regulators of T-cell fate: integration of cell migration, differentiation and function. *Immunol Rev* 2019; **289**: 101–114.
3. Groom JR, Luster AD. CXCR3 ligands: redundant, collaborative and antagonistic functions. *Immunol Cell Biol* 2011; **89**: 207–215.
4. Groom JR, Richmond J, Murooka TT, *et al.* CXCR3 chemokine receptor-ligand interactions in the lymph node optimize $CD4^+$ T helper 1 cell differentiation. *Immunity* 2012; **37**: 1091–1103.
5. Hu JK, Kagari T, Clingan JM, Matloubian M. Expression of chemokine receptor CXCR3 on T cells affects the balance between effector and memory CD8 T-cell generation. *Proc Natl Acad Sci USA* 2011; **108**: E118–E127.
6. Kohlmeier JE, Reiley WW, Perona-Wright G, *et al.* Inflammatory chemokine receptors regulate $CD8^+$ T cell contraction and memory generation following infection. *J Exp Med* 2011; **208**: 1621–1634.
7. Kurachi M, Kurachi J, Suenaga F, *et al.* Chemokine receptor CXCR3 facilitates $CD8^+$ T cell differentiation into short-lived effector cells leading to memory degeneration. *J Exp Med* 2011; **208**: 1605–1620.
8. Duckworth BC, Lafouresse F, Wimmer VC, *et al.* Effector and stem-like memory cell fates are imprinted in distinct lymph node niches directed by CXCR3 ligands. *Nat Immunol* 2021; **22**: 434–448.
9. Campanella GS, Medoff BD, Manice LA, Colvin RA, Luster AD. Development of a novel chemokine-mediated *in vivo* T cell recruitment assay. *J Immunol Methods* 2008; **331**: 127–139.
10. Campanella GS, Tager AM, El Khoury JK, *et al.* Chemokine receptor CXCR3 and its ligands CXCL9 and CXCL10 are required for the development of murine cerebral malaria. *Proc Natl Acad Sci USA* 2008; **105**: 4814–4819.
11. Kohlmeier JE, Cookenham T, Miller SC, *et al.* CXCR3 directs antigen-specific effector $CD4^+$ T cell migration to the lung during parainfluenza virus infection. *J Immunol* 2009; **183**: 4378–4384.
12. Cole KE, Strick CA, Paradis TJ, *et al.* Interferon-inducible T cell α chemoattractant (I-TAC): a novel non-ELR CXC chemokine with potent activity on activated T cells through selective high affinity binding to CXCR3. *J Exp Med* 1998; **187**: 2009–2021.
13. Lee HH, Farber JM. Localization of the gene for the human MIG cytokine on chromosome 4q21 adjacent to INP10 reveals a chemokine "mini-cluster". *Cytogenet Cell Genet* 1996; **74**: 255–258.
14. Erdel M, Theurl M, Meyer M, Duba HC, Utermann G, Werner-Felmayer G. High-resolution mapping of the human 4q21 and the mouse 5E3 SCYB chemokine cluster by fiber-fluorescence in situ hybridization. *Immunogenetics* 2001; **53**: 611–615.
15. Colvin RA, Campanella GS, Sun J, Luster AD. Intracellular domains of CXCR3 that mediate CXCL9, CXCL10, and CXCL11 function. *J Biol Chem* 2004; **279**: 30219–30227.
16. Sauty A, Colvin RA, Wagner L, Rochat S, Spertini F, Luster AD. CXCR3 internalization following T cell-endothelial cell contact: preferential role of IFN-inducible T cell α chemoattractant (CXCL11). *J Immunol* 2001; **167**: 7084–7093.
17. Zohar Y, Wildbaum G, Novak R, *et al.* CXCL11-dependent induction of FOXP3-negative regulatory T cells suppresses autoimmune encephalomyelitis. *J Clin Invest* 2014; **124**: 2009–2022.
18. Clark-Lewis I, Mattioli I, Gong JH, Loetscher P. Structure-function relationship between the human chemokine receptor CXCR3 and its ligands. *J Biol Chem* 2003; **278**: 289–295.
19. Groom JR, Luster AD. CXCR3 in T cell function. *Exp Cell Res* 2011; **317**: 620–631.
20. Woodruff MC, Heesters BA, Herndon CN, *et al.* Trans-nodal migration of resident dendritic cells into medullary interfollicular regions initiates immunity to influenza vaccine. *J Exp Med* 2014; **211**: 1611–1621.
21. Sung JH, Zhang H, Moseman EA, *et al.* Chemokine guidance of central memory T cells is critical for antiviral recall responses in lymph nodes. *Cell* 2012; **150**: 1249–1263.
22. Kastenmuller W, Brandes M, Wang Z, Herz J, Egen JG, Germain RN. Peripheral prepositioning and local CXCL9 chemokine-mediated guidance orchestrate rapid memory $CD8^+$ T cell responses in the lymph node. *Immunity* 2013; **38**: 502–513.

23. Ali A, Canaday LM, Feldman HA, *et al*. Natural killer cell immunosuppressive function requires CXCR3-dependent redistribution within lymphoid tissues. *J Clin Invest* 2021; **131**: e146686.
24. Sierro F, Biben C, Martinez-Munoz L, *et al*. Disrupted cardiac development but normal hematopoiesis in mice deficient in the second CXCL12/SDF-1 receptor, CXCR7. *Proc Natl Acad Sci USA* 2007; **104**: 14759–14764.
25. Qi Z, Wang J, Han X, Yang J, Zhao G, Cao Y. *Listr1* locus regulates innate immunity against *Listeria monocytogenes* infection in the mouse liver possibly through *Cxcl11* polymorphism. *Immunogenetics* 2014; **66**: 231–242.
26. Burns JM, Summers BC, Wang Y, *et al*. A novel chemokine receptor for SDF-1 and I-TAC involved in cell survival, cell adhesion, and tumor development. *J Exp Med* 2006; **203**: 2201–2213.
27. Infantino S, Moepps B, Thelen M. Expression and regulation of the orphan receptor RDC1 and its putative ligand in human dendritic and B cells. *J Immunol* 2006; **176**: 2197–2207.
28. Humpert ML, Pinto D, Jarrossay D, Thelen M. CXCR7 influences the migration of B cells during maturation. *Eur J Immunol* 2014; **44**: 694–705.
29. Benredjem B, Girard M, Rhainds D, St-Onge G, Heveker N. Mutational analysis of atypical chemokine receptor 3 (ACKR3/CXCR7) interaction with its chemokine ligands CXCL11 and CXCL12. *J Biol Chem* 2017; **292**: 31–42.
30. Karin N, Wildbaum G, Thelen M. Biased signaling pathways via CXCR3 control the development and function of $CD4^+$ T cell subsets. *J Leukoc Biol* 2016; **99**: 857–862.
31. Sanchez-Martin L, Sanchez-Mateos P, Cabanas C. CXCR7 impact on CXCL12 biology and disease. *Trends Mol Med* 2013; **19**: 12–22.
32. Singh AK, Arya RK, Trivedi AK, *et al*. Chemokine receptor trio: CXCR3, CXCR4 and CXCR7 crosstalk via CXCL11 and CXCL12. *Cytokine Growth Factor Rev* 2013; **24**: 41–49.
33. Marsman C, Lafouresse F, Liao Y, *et al*. Plasmacytoid dendritic cell heterogeneity is defined by CXCL10 expression following TLR7 stimulation. *Immunol Cell Biol* 2018; **96**: 1083–1094.
34. Piovesan D, Tempany J, Di Pietro A, *et al*. c-Myb regulates the T-Bet-dependent differentiation program in B cells to coordinate antibody responses. *Cell Rep* 2017; **19**: 461–470.
35. Ryg-Cornejo V, Ioannidis LJ, Ly A, *et al*. Severe malaria infections impair germinal center responses by inhibiting T follicular helper cell differentiation. *Cell Rep* 2016; **14**: 68–81.
36. Ly A, Liao Y, Pietrzak H, *et al*. Transcription factor T-bet in B cells modulates germinal center polarization and antibody affinity maturation in response to malaria. *Cell Rep* 2019; **29**: e2256.
37. Boldajipour B, Mahabaleshwar H, Kardash E, *et al*. Control of chemokine-guided cell migration by ligand sequestration. *Cell* 2008; **132**: 463–473.
38. Sheikh AA, Cooper L, Feng M, *et al*. Context-dependent role for T-bet in T follicular helper differentiation and germinal center function following viral infection. *Cell Rep* 2019; **28**: e1754.
39. Mendoza A, Yewdell WT, Hoyos B, *et al*. Assembly of a spatial circuit of T-bet-expressing T and B lymphocytes is required for antiviral humoral immunity. *Sci Immunol* 2021; **6**: eabi4710.
40. Duckworth BC, Groom JR. Conversations that count: cellular interactions that drive T cell fate. *Immunol Rev* 2021; **300**: 203–219.
41. De Giovanni M, Cutillo V, Giladi A, *et al*. Spatiotemporal regulation of type I interferon expression determines the antiviral polarization of $CD4^+$ T cells. *Nat Immunol* 2020; **21**: 321–330.
42. Dufour JH, Dziejman M, Liu MT, Leung JH, Lane TE, Luster AD. IFN-γ-inducible protein 10 (IP-10; CXCL10)-deficient mice reveal a role for IP-10 in effector T cell generation and trafficking. *J Immunol* 2002; **168**: 3195–3204.
43. Park MK, Amichay D, Love P, *et al*. The CXC chemokine murine monokine induced by IFN-γ (CXC chemokine ligand 9) is made by APCs, targets lymphocytes including activated B cells, and supports antibody responses to a bacterial pathogen *in vivo*. *J Immunol* 2002; **169**: 1433–1443.
44. Vanden Berghe T, Hulpiau P, Martens L, *et al*. Passenger mutations confound interpretation of all genetically modified congenic mice. *Immunity* 2015; **43**: 200–209.
45. Puchert M, Obst J, Koch C, Zieger K, Engele J. CXCL11 promotes tumor progression by the biased use of the chemokine receptors CXCR3 and CXCR7. *Cytokine* 2020; **125**: 154809.
46. Majumdar S, Murphy PM. Adaptive Immunodeficiency in WHIM Syndrome. *Int J Mol Sci* 2018; **20**: 3.

SUPPORTING INFORMATION

Additional supporting information may be found online in the Supporting Information section at the end of the article.